On the transformation of Pacific Water into Indonesian Throughflow Water by internal tidal mixing

Ariane Koch-Larrouy,[1] Gurvan Madec,[1] Pascale Bouruet-Aubertot,[1] Theo Gerkema,[2] Laurent Bessières,[3] and Robert Molcard[1]

Received 10 October 2006; revised 18 November 2006; accepted 16 January 2007; published 21 February 2007.

[1] The Indonesian archipelago is characterized by strong internal tides, which are trapped in the different semi-enclosed seas of the archipelago. Using tidal model results a parameterization of the associated 3d tidal mixing is developed. The resulting average vertical diffusivity is 1.5 cm^2/s, which independently agrees with the estimates inferred from observations. Introduced in a regional OGCM, the parameterization improves the water mass characteristics in the different Indonesian seas, suggesting that the horizontal and vertical distributions of the mixing are adequately prescribed. In particular, the salinity maximum of the inflow water is reduced along the main route, mainly in the Dewakang sill area. But also it is erased in the Halmahera and Seram seas, the entrance of the eastern route, so that salty waters doesn't penetrate the Banda Sea. As a result the simulated Indonesian Throughflow Water are in good agreement with observations. **Citation:** Koch-Larrouy, A., G. Madec, P. Bouruet-Aubertot, T. Gerkema, L. Bessières, and R. Molcard (2007), On the transformation of Pacific Water into Indonesian Throughflow Water by internal tidal mixing, *Geophys. Res. Lett.*, *34*, L04604, doi:10.1029/2006GL028405.

1. Introduction

[2] The Indonesian Throughflow (ITF) is the only low-latitude passage between two oceans. Due to its strategic position, it plays an important role in the global ocean and climate regulation [*Hirst and Godfrey*, 1993; *Wajsowicz and Schneider*, 2001]. The ITF is divided into three main branches that advect either north or south Pacific waters. The main route drives North Pacific water, characterized by a salinity maximum (34.8 psu, North Pacific Subtropical Water, NPSW, black curve box 1 (Figure 1)), through the Sulawesi Sea and the Makassar Strait, and exits through the Lombok and Ombai Straits and through the Timor Passage (Figure 1) [*Gordon and Fine*, 1996]. About 90% of the ITF thermocline water flows through this main route with an estimated transport of 10 ± 5 Sv ($1\ Sv = 10^6\ m^3/s$) [*Gordon*, 2005]. The second route advects subthermocline water of South Pacific origin through the Maluku Sea and the Lifamatola Strait. It has a transport of $\sim 1.5-3$ Sv [*Van Aken et al.*, 1988; *Gordon et al.*, 2003]. South Pacific waters characterized by a higher salinity maximum around 35.45 psu (South Pacific Subtropical Water, SPSW, black curve box 4 (Figure 1)) flow through the last route passing by the Halmahera, Seram and Banda Seas [*Gordon and Fine*, 1996]. About 10% of the thermocline water is advected by this last branch with a transport of ~ 1 or 2 Sv inferred from the balance between the exit and the entrance [*Gordon*, 2005].

[3] In the Banda Sea, where the two routes of thermocline waters converge, there is no more signature of the two salinity maxima. Instead, transformations of these Pacific incoming waters has led to a unique water mass that has a constant salinity below 20°C (34.58 psu, box 8 (Figure 1)).

[4] Several studies suggest that internal tides are responsible for the intense mixing required for this transformation in the ITF region [*Schiller*, 2004; *Hatayama*, 2004; *Robertson and Ffield*, 2005]. The *Carrère and Lyard* [2003] model gives the amount of energy transferred from barotropic tides to baroclinic tides, which is particularly strong in this area (Figure 1, middle plot). Over the Indonesian semi-enclosed seas 0.11 TW is transferred, which represent 10% of the energy transfer in the global ocean (1.1 TW) for a surface of 0.5% of the entire ocean. So the energy transfer averaged over this area is 20 times higher per unit of area than the averaged value over the entire ocean.

[5] The mean vertical diffusivity required to reproduce the observed water mass transformations has been estimated using an advection-diffusion model to be $1-2\ cm^2/s$ [*Ffield and Gordon*, 1992; *Hautala et al.*, 1996]. However, this value is deduced from a T-S budget over the whole area and cannot describe the spatial distribution of mixing. A few sets of measurements and numerical experiments suggested that mixing is highly variable in the Indonesian seas with clear enhancement at sills and continental shelves (up to 60 cm^2/s) [*Hatayama*, 2004], as opposed to the sub-basins interiors (0.09 cm^2/s) [*Alford et al.*, 1999; *Ffield and Robertson*, 2005; *Robertson and Ffield*, 2005]. Nevertheless the precise locations of water mass transformations remain unclear.

[6] This study investigates the role of internal tidal mixing on water mass transformation in the archipelago sub-basins. With this purpose an OGCM (section 3) is used with a specific parameterization that mimics the internal tide effect in this particular region (described in section 2). The main results about where this tidal mixing occurs and how it affects water masses are presented in section 4. Conclusions are given in section 5.

2. Tidal Mixing Parameterization

[7] Our parameterization of tidal mixing follows the general formulation for the vertical eddy diffusivity pro-

[1]Laboratoire d'Océanographie et du Climat, Laboratoire d'Océanographie Dynamique et de Climatologie, Paris, France.
[2]Royal Netherlands Institute for Sea Research, Den Burg, Netherlands.
[3]Laboratoire d'Etudes en Géophysique et Océanographie Spatiale, Toulouse, France.

0094-8276/07/2006GL028405

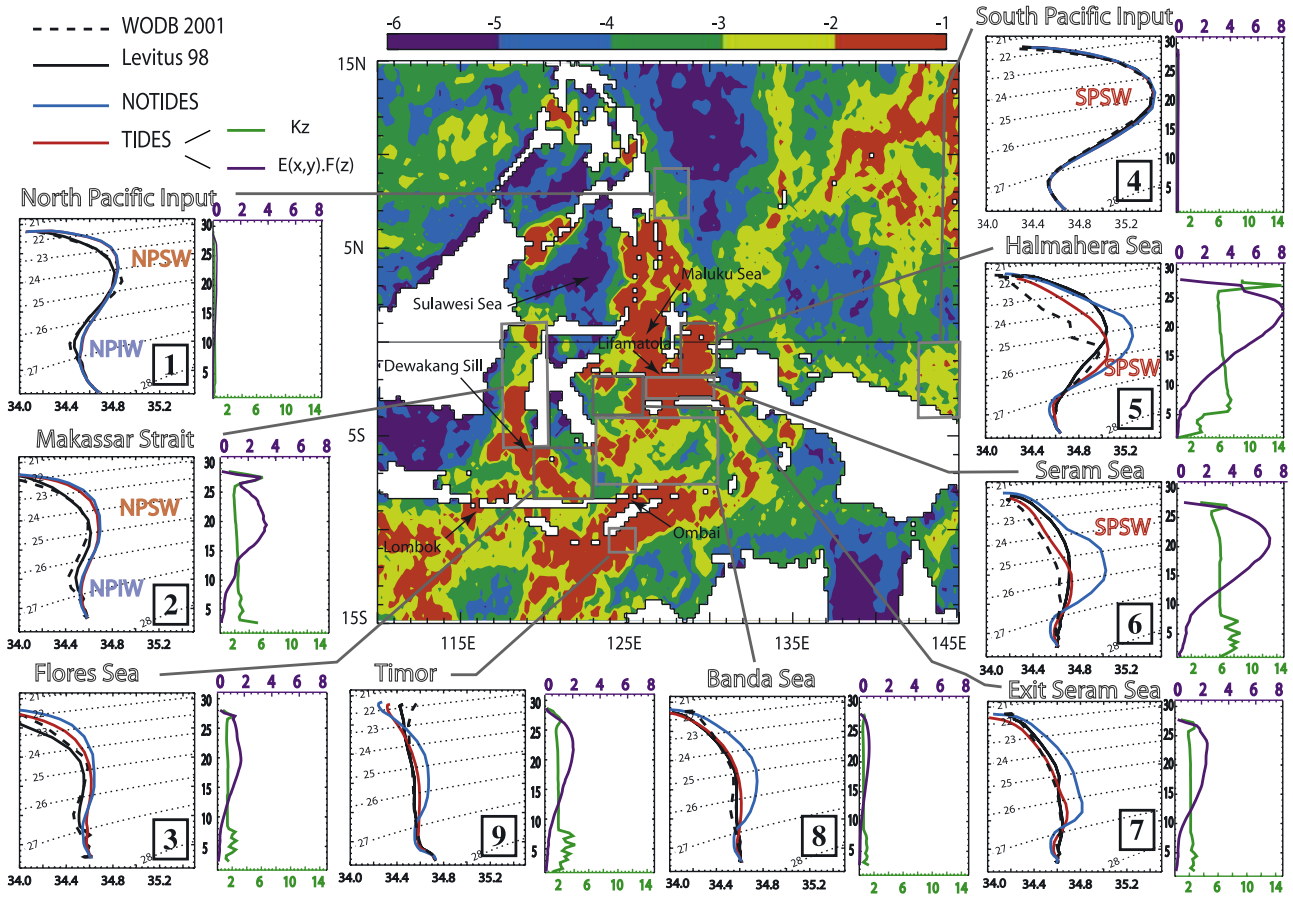

Figure 1. Map of barotropic to baroclinic tides energy transfer (E) from the *Carrère and Lyard* [2003] model (logarithmic scaling, TW/m^2). Significant vertical diffusivity is only generated in the red patches. Plots show horizontally averaged properties in the 9 boxes indicated on the map: (left) T-S diagram of the World Ocean Data Base 2001 (solid black line), *Levitus et al.* [1998] (dashed black line), NOTIDES (blue line), and TIDES (red line) and (right) vertical profile of the energy transfer [$E(x,y).F(z)$] (purple) given in 10^{-4} TW/m^3 and the vertical diffusivity (green) given in cm^2/s. Vertical scale is the temperature.

posed by *St. Laurent et al.* [2002] and implemented by L. Bessières et al. (Improved tidally driven mixing in a numerical model of the ocean general circulation, submitted to *Ocean Modeling*, 2006) in the OGCM used in this study. In this formulation the vertical diffusivity resulting from internal tide breaking, k_{tides} is expressed as a function of the energy transfer from barotropic tides to baroclinic tides which is a function of space and stratification:

$$k_{tides} = \frac{q\Gamma E(x,y)F(z)}{\rho N^2} \qquad (1)$$

Where $\Gamma = 0.2$ is the mixing efficiency, N the Brunt-Väisälä frequency, ρ the density, q the tidal dissipation efficiency, $E(x,y)$ the energy transfer per unit of area from barotropic tides to baroclinic tides and $F(z)$ its vertical structure.

[8] In this formulation three key parameters have been adjusted to the ITF region: q, $E(x,y)$, $F(z)$.

[9] 1. The Indonesian archipelago is a complex geographic region with a series of large, deep, semi-enclosed basins connected via numerous narrow straits. Once generated, internal tides remain confined within this semi-enclosed area and hardly radiate away. Therefore all the internal tides energy is consumed within this area. So it is assumed that $q = 1$.

[10] 2. $E(x,y)$ has been inferred from a finite element barotropic ocean tidal model [*Le Provost et al.*, 1994; *Carrère and Lyard*, 2003]. Four main regions of high energy transfer can be distinguished on the map displayed in Figure 1 (middle plot): In the eastern route (Halmahera, Seram and Maluku Seas) 4.1 10^{-2} TW (40% of the energy within the semi-enclosed seas) is dissipated. The western route (Makassar, Flores Seas), accounts for 2.4 10^{-2} TW (21%). The Timor Passage accounts for 1.9 10^{-2} TW (17%). Finally, in the entrance of the Sulawesi Sea 1.1 10^{-2} TW (10%) is converted. The energy distribution is therefore highly heterogeneous with clear enhancement before and after the Banda Sea.

[11] Once generated the internal tides propagate and remain confined in each semi-enclosed sea where they have been generated. We successively tested applying either the mean $E(x,y)$ over each semi-enclosed sea or the local value of $E(x,y)$. The transformation of the water mass remains unchanged. In the following we use for $E(x,y)$ the energy transfer displayed in Figure 1.

[12] 3. The vertical distribution of the energy dissipation, $F(z)$, is a key point of the parameterization. This distribution

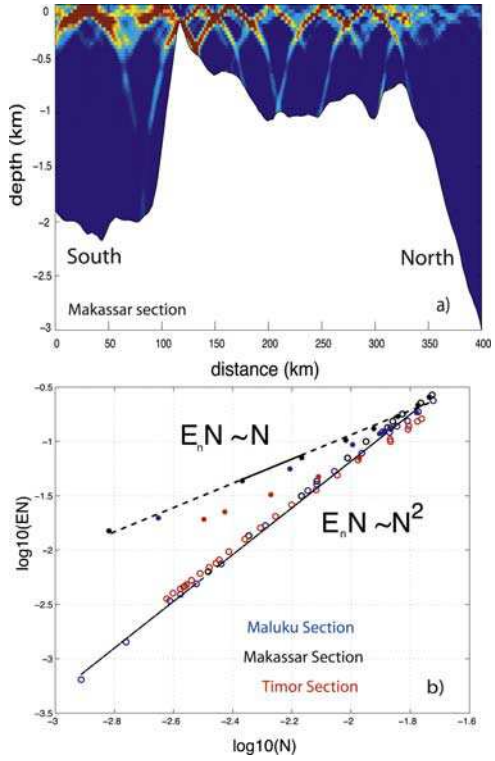

Figure 2. (a) Vertical section of the energy of the semi-diurnal, M2, baroclinic tide along the Maluku Strait vertical section. (b) E_nN as a function of N in (*log*, *log*) coordinates for the Maluku Sea, the Makassar and Timor straits vertical sections; E_nN scales like N^2 in the ocean interior up to the depth of maximum of N^2 and scales like N above.

depends on the specificities of internal-tide generation and thus can vary strongly from one region to another. In order to determine the vertical distribution of internal tides (and hence that of their induced dissipation and mixing), an internal-tide generation model [*Gerkema et al.*, 2004] was applied to several vertical sections in the most important straits of the ITF. The model involves a 3D velocity field, but assumes full uniformity in the along-slope direction. The forcing mechanism involves three ingredients which need to be prescribed: the barotropic cross-slope flux, the topographic profile (uniformity is assumed in the along-slope direction), and the buoyancy frequency $N(z)$. The model is linear and hydrostatic, in the horizontal cross-slope direction a fourth-order central-difference scheme is used (resolution of 400 m), in the vertical a Chebyshev collocation method is used involving 60 polynomials. Time-integration is done using a third-order Adams-Bashforth scheme. We start from rest and carry out a calculation over 20 tidal periods; by the end, all transients have left the domain of interest, and have been absorbed by sponge layers placed at the outer ends.

[13] The bathymetry was inferred from the TOPEX dataset (http://topex.ucsd.edu/cgi-bin/get_data.cgi). Buoyancy frequency is set from observations and the barotropic cross-slope flux is arbitrarily prescribed to a constant value. The two dominant tidal components, $M2$ and $K1$, are used separately. An example of the spatial distribution of the tidal energy is shown in Figure 2a for the semi-diurnal $M2$ baroclinic tide along the Makassar Strait vertical section. The baroclinic tide is mainly generated where the bottom slope is critical (i.e. corresponds to the direction of propagation of the baroclinic tide).

[14] The purpose is to provide a vertical profile of energy dissipation, namely $F(z)$ in equation (1), inferred from the spatial distribution of the energy of the baroclinic tide. It is assumed that the energy dissipation scales like E_nN, where E_n is the energy of the baroclinic tide. In doing so, the typical time scale for energy dissipation is set to be $1/N$. The physical argument behind this scaling is that the duration of wavebreaking events scales with the smallest period of internal waves. This parameterization of energy dissipation is consistent with that presented by *D'Asaro and Lien* [2000] for high energy level of the internal wave field.

[15] The depth dependence of the energy dissipation, and more precisely $F(z)$, is inferred from the vertical profile of E_nN: $F(z) = E_nN/\int E_nN\, dz$, which is then substituted into equation (1).

[16] Alternatively one could look for a formulation of the energy dissipation as a function of the stratification alone, which would allow to deal with varying stratification during the numerical simulation. These two quantities are displayed in Figure 2b. Interestingly two scaling laws were found depending on the sign of the vertical gradient of N: $E_nN \sim N$ when $dN/dz < 0$ (above the core of the thermocline) and $E_nN \sim N^2$ when $dN/dz > 0$, which are then substituted into equation (1):

$$k_{tides} = \begin{cases} q\Gamma E(x,y)/\left(\rho \int N^2 dz\right) \text{ when } dN/dz < 0 \\ q\Gamma E(x,y)/\left(\rho N \int N^2 dz\right) \text{ when } dN/dz > 0. \end{cases} \quad (2)$$

Figure 1 displays the key parameters involved in the parameterization: $E(x,y)$, the vertical profiles horizontally averaged over different boxes of the energy transfer $[E(x,y).F(z)]$ and of the eddy diffusivity kz. The profile of the energy transfer is maximum in the thermocline. On the lower part of the thermocline and below the vertical diffusivity becomes uniform on the vertical (equation (2)). The irregularities near the bottom are only due to the average on the vertical of ocean water columns that do not have the same depth. In the regions of strong concentration (Seram and Halmahera Seas, Makassar Strait, Timor passage), the averaged energy reaches its maximum in the thermocline (2.10^{-4} to 8.10^{-4} TW). Averaged vertical diffusivities reach values of a few cm^2/s, with a maximum of a dozens of cm^2/s above sills in agreement with *Hatayama* [2004]. The vertical diffusivity averaged over all the semi-enclosed seas is about 1.5 cm^2/s. This result based on tidal energy constrain is in very good agreement with the estimation of advection diffusion model based on independent data set [*Ffield and Gordon*, 1992; *Hautala et al.*, 1996]. This suggests that the tides energy is a major source of energy to explain the strong vertical diffusivity found in the Indonesian region.

3. Ocean Model Configuration

[17] The model configuration is a sub-domain of the global ocean model ORCA025 described by *Barnier et al.*

[2006]. It uses the latest version of the NEMO/OPA Ocean General Circulation model (G. Madec, NEMO = the OPA9 ocean engine, note du pole de modelisation, 2006, Institut Pierre-Simon Laplace, available at http://www.lodyc.jussieu.fr/NEMO/). The model has a 0.25° horizontal resolution with eddy resolving capabilities which is a good compromise between CPU consumption and complex strait configuration. The vertical grid has 46 levels, with a resolution ranging from 5 m at the surface to 250 m at the bottom. Partial step for bathymetry modeling has been implemented. The background vertical diffusivity is 0.1 cm^2/s. The domain extends from 95°E to 145°E in longitude and from 25°S to 25°N in latitude. Open boundary conditions are provided by the reference simulation ORCA025 [*Barnier et al.*, 2006]. The model is forced by daily climatological wind stress fields derived weekly from the European Remote Sensing satellites (ERS) during the period 1992–2001. Surface heat fluxes and evaporation are computed with bulk formulas using climatologies from the ERS satellites and the Climate Prediction Center Merged Analysis of Precipitation (NCEP/NCAR) for surface air temperature, specific humidity and observational climatology of cloud cover. The surface fresh water flux is derived from the CMAP precipitation maps to which is added a weak relaxation to the surface salinity of *Levitus et al.* [1998].

[18] To investigate the influence of the tidal mixing parameterization on the water mass transformation in the Indonesian region, two 10-year simulations were performed that only differ by the vertical mixing parameterization: NOTIDES (without the tidal mixing parameterization), TIDES (with the tidal mixing parameterization). Two additional experiments were performed in order to isolate the influence of tidal mixing along the western route and the eastern routes: TIDES-E (with tidal mixing parameterization only on the eastern route), TIDES-W (with the tidal mixing parameterization only in the western route).

4. Results

[19] In terms of transport, the TIDES and NOTIDES experiments are roughly identical (no more than 5% differences). In both, the total transport (16.6 Sv) is 30% larger than the observed estimates (10 ± 5 Sv) but is in good agreement with the Island Rule calculation [*Godfrey*, 1989] applied to the model wind stress forcing. The paths within the Indonesian archipelago are well represented by the model. The major route is passing through the Makassar strait with a North Pacific origin. The transport through the 3 exits and their relative balance compares well with observations, even if they are 10–40% larger than observed: 2.6, 6.3, 7.7 Sv vs. 1.7, 4.3, 4.5–7 Sv, for the Lombok Strait [*Arief and Murray*, 1996], the Ombai Strait [*Molcard et al.*, 2001], and the Timor Passage [*Molcard et al.*, 1996; *Cresswell et al.*, 1993] respectively. Part of the flow recirculates west of Banda Sea before exiting through the Timor passage. On the eastern route, a deep flow enters the Indonesian seas from the South Pacific (2.6 Sv) and from the North Pacific (1.8 Sv) via Maluku and Lifamatola Strait (50% larger than in the work of *Gordon et al.* [2003]). Furthermore, annual transport via the last route, advecting thermocline water from South Pacific Ocean through the Halmahera and Seram Seas is 0.25 Sv in the surface layer, almost zero in the density range of the salinity maximum of the SPSW, and 0.25 Sv in the density range of the South Pacific Central Water. Seasonally, the flow reverses and, all along the year, eddies induce large recirculations. In the upper thermocline, maximum southward transport occurs in April whereas for the lower thermocline the flow is southward from October to February with a value that does not exceed 1 Sv. The transport along this route is slightly underestimated (0.5 Sv) compared to the value of 1 Sv deduced from observation [*Gordon*, 2005].

[20] Even though the transports are similar, the water mass transformation strongly differs in the TIDES and NOTIDES experiments. The water mass transformation is shown in Figure 1 which displays observed and simulated T-S diagram in several sub-basins along the pathways within the Indonesian archipelago. In the observations, the North and South Pacific subtropical salinity maxima are attenuated all along their respective western and eastern route (black curves in Figure 1). In particular the SPSW salinity maximum is strongly eroded from its entrance in the Halmahera Sea (box 5, Figure 1) and vanishes in the Seram Sea (box 6–7, Figure 1). Therefore, these observational results clearly show that this mixing of the SPSW happened before entering the Banda Sea. The NOTIDES experiment cannot reproduce these transformations; the SPSW salinity maximum signature is still visible in the Seram and Banda Seas in opposition to what is observed. In contrast, the TIDES run reproduces well the transformations in all the sub-basins, eroding the subtropical salinity maximum of the western and eastern route as observed. It leads to a significant improvement of the outflow in the Timor Passage. Results from TIDES-W and TIDES-E (not shown) reveal that half of this improvement is due to the transformation in the western route and the other half to the transformation in the eastern route, suggesting that mixing in both routes has its importance in setting the water mass characteristics even though the respective transports differ strongly.

[21] For the western route, the North Pacific water mass presents a bias (box 1, Figure 1) at the entrance still visible within the Makassar Strait and the Flores Sea. The maximum of salinity is progressively eroded in Makassar Strait and in Flores Sea. The salt content is conserved and redistributed on the vertical. This route receives 21% of the tidal energy of all the semi-enclosed seas (0.024 TW). This generates a mean vertical diffusivity of 1 to 2 cm^2/s in the thermocline with local maximum of 14 cm^2/s above Dewakang Sill (separating the southern Makassar Strait from the Flores Sea). This improves the profiles in the Flores Sea (box 3). Figure 3, which displays the salinity in the upper and lower thermocline for both TIDES and NOTIDES experiments, points out the particular role of the Dewakang Sill on the water masses transformation. Along the upper western route, the salinity decreases due to strong vertical mixing at the Dewakang Sill (34.65 psu in NOTIDES, to 34.58 psu in TIDES run (Figure 3)). This causes the salinity difference in the Southwest Banda Sea between the two experiments. The salinity change is weak but it concerns 90% of the ITF thermocline water. Therefore, this confirms *Hatayama*'s [2004] results that demon-

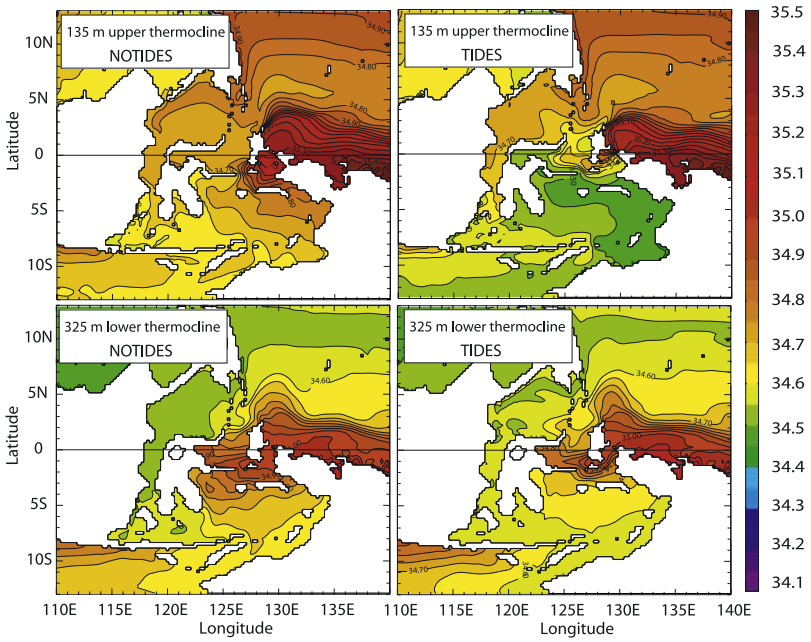

Figure 3. Salinity in the upper and lower thermocline for the TIDES and NOTIDES run.

strated the major role of the Dewakang Sill in water masses transformation induced by vertical tidal mixing.

[22] On the eastern route, the effect of internal tidal mixing is even more striking than for the western route. The South Pacific water mass at the entrance is reproduced in good agreement with observations (box 4, Figure 1). In the Halmahera and Seram Seas (boxes 5–6), the available tidal energy is greater than 0.041 TW (Figure 1, middle plot) representing 40% of the energy contained in the semi-enclosed seas of the archipelago. This generates an averaged vertical diffusivity as high as 6 cm^2/s with a local maximum of 14 cm^2/s in the thermocline. This mixing reduces the salinity maximum in the Halmahera Sea from 35.2 psu (NOTIDES run) to 35.0 psu (TIDES run) and in Seram Sea from 35.0 to 34.7, in good agreement with observations (black curves). At the Seram Sea exit (box 7, Figure 1) and in the TIDES experiment, the water column has no more signature of the SPSW, as observed. Therefore, the transformation of the SPSW clearly occurs before the Banda Sea. Furthermore, within the Banda Sea, the average vertical diffusivity is weak, with values of about 0.3 cm^2/s and a local maximum that does not exceed 0.5 cm^2/s. This suggests that the Banda Sea does not play an important role in vertical mixing for either route since the energy is much higher before entering this Sea.

[23] Figure 3 illustrates the invasion in the Banda Sea of South Pacific salty waters when no enhanced tidal mixing parameterization (NOTIDES experiment). Indeed, without any specific representation of vertical mixing, the eastern route pollutes the upper thermocline of the Banda Sea and the Timor exit with salty water, despite the relatively weak transport along this route. Using the tidal vertical parameterization (TIDES experiment) prevents such a penetration (Figure 3). The salt content of the Banda Sea is partly redistributed on the vertical but also is reduced. Indeed tidal mixing erases the salinity maximum at the entrance of Halmahera Sea in the core of the southward baroclinic flow (not shown). Some of the salt contained in the SPSW is redistributed in the vertical without entering the Indonesian Seas. Moreover the rest of the salty water from SPSW remains confined in the Seram Sea in good agreement with *Gordon* [2005, Figure 3D]. In addition, the lower thermocline in the Banda Sea is also improved by vertical mixing, with the signature of the salty waters from the SPSW still visible, in good agreement with observations [*Gordon*, 2005].

[24] The Banda Sea salinity characteristics are therefore strongly influenced by the eastern route, even if its associated transport is weaker than its western counterpart. The mixing in the Halmahera and Seram Seas controls the salinity in the Banda Sea and the effect of vertical tidal mixing plays a major role in determining the T-S profiles in that area and in the Timor Passage (TIDES-E, not shown).

5. Conclusion

[25] The role of tidal vertical mixing on water mass transformation in the ITF has been investigated using a set of regional OGCM simulations. In this region, the energy transfer from barotropic tides to baroclinic tides, E, is highly heterogeneous and its area mean magnitude is 20 times higher than for the global ocean. Moreover the ITF is a unique area where this strong internal tidal energy hardly radiates away due to the existence of multiple semi-enclosed seas, and remains confined. Based on *St. Laurent et al.*'s [2002] work, we developed a specific parameterization to mimic the internal tides effect in this particular region. The parameterization relies on the following 3 points: (1) all the energy generated is available for mixing; (2) the horizontal distribution of the energy dissipation is constrained by E provided by the *Carrère and Lyard* [2003] tidal model results. (3) Using a 2D linear model of internal

tide generation [*Gerkema et al.*, 2004] applied to several vertical section of the Indonesian straits, the vertical distribution of the energy dissipation is found to be proportional to N^2 below the core of the thermocline and to N above. The model results show a maximum of energy dissipation within the thermocline. The resulting vertical diffusivities vary from a few cm^2/s to a dozen of cm^2/s. The vertical diffusivity is constant bellow the core of the thermocline and its average over the semi-enclosed seas is 1.5 cm^2/s, in good agreement with the independent estimation of *Ffield and Gordon* [1992], who used an advection diffusion model. This agreement suggests that the tidal energy is a major source of energy to explain the strong transformation of Pacific water mass within the Indonesian archipelago. When applying the parameterization in the ¼° OGCM used here, the T-S properties in all the Indonesian basins, are considerably improved and reach a good agreement with in situ observations. This suggests that the spatial distribution of the vertical diffusivity is adequately prescribed and able to reproduce the heterogeneity of the mixing. In particular, 20% of the tidal energy is dissipated along the western route and related to the very localized transformation that occurs in the vicinity of the Dewakang Strait. The associated salinity change is relatively modest, but it significantly influences the T-S characteristics at the exits of the archipelago as it involves 90% of the flow in the thermocline. Furthermore, 40% of the tidal energy is concentrated in the Halmahera and Seram Seas where a major improvement of the water mass occurs. Indeed, even if it concerns a minor pathway its impact on the Banda Sea and the Indonesian Throughflow Water T-S characteristics is predominant.

[26] **Acknowledgments.** We thank the DRAKKAR project and in particular Anne-Marie Tréguier for the ITF configuration and data at open boundaries condition. We also thank F. Lyard and the late and regretted C. Le Provost for providing the outputs from the Tidal model. We thank Agus Atmadipoera and Matthieu Lengaigne for fruitful discussions. This work is supported by MERCATOR-ocean (projects 100043 and 061396) and by the Marine Environement and Security for the European Area project (MERSEA, SIP3 CI 2003 502885). The ocean model integrations have been performed at the Institut de Développement et des Ressources en Informatique Scientifique (IDRIS, project 51140 and 1396). P. Bouruet-Aubertot acknowledges the Royal Netherlands Institute for Sea Research for financial support to this collaboration. Theo Gerkema is supported by the NOW/ALW program CLIMA-DIM.

References

Alford, M. H., M. C. Gregg, and M. Ilyas (1999), Diapycnal mixing in the Banda Sea: Results of the first microstructure measurements in the Indonesian Throughflow, *Geophys. Res. Lett.*, *26*(17), 2741–2744.

Arief, D., and S. P. Murray (1996), Low-frequency fluctuations in the Indonesian throughflow through Lombok Strait, *J. Geophys. Res.*, *101*, 12,455–12,464.

Barnier, B., et al. (2006), Impact of partial steps and momentum advection schemes in a global ocean circulation model at eddy permitting resolution, *Ocean Dyn.*, *56*, 377–378, doi:10.1007/s10236-006-0090-1.

Carrère, L., and F. Lyard (2003), Modeling the barotropic response of the global ocean to atmospheric wind and pressure forcing: Comparisons with observations, *Geophys. Res. Lett.*, *30*(6), 1275, doi:10.1029/2002GL016473.

Cresswell, G., A. Frische, J. Peterson, and D. Quadfasel (1993), Circulation in the Timor Sea, *J. Geophys. Res.*, *98*, 14,379–14,389.

D'Asaro, E. A., and R. C. Lien (2000), The wave-turbulence transition for stratified flows, *J. Phys. Oceanogr.*, *30*, 1669–1678.

Ffield, A., and A. L. Gordon (1992), Vertical mixing in the Indonesian thermocline, *J. Phys. Oceanogr.*, *22*, 184–195.

Ffield, A., and R. Robertson (2005), Indonesian Seas fine structure variability, *Oceanography*, *18*, 108–111.

Gerkema, T., F.-P. A. Lam, and L. R. M. Maas (2004), Internal tides in the Bay of Biscay: Conversion rates and seasonal effects, *Deep Sea Res., Part II*, *51*, 2995–3008.

Godfrey, J. S. (1989), A Sverdrup model of the depth-integrated flow for the world ocean allowing for island circulations, *Geophys. Astrophys. Fluid Dyn.*, *45*, 89–112.

Gordon, A. L. (2005), Oceanography of the Indonesian seas and their throughflow, *Oceanography*, *18*, 14–27.

Gordon, A. L., and R. A. Fine (1996), Pathways of water between the Pacific and Indian oceans in the Indonesian seas, *Nature*, *379*(6561), 146–149.

Gordon, A. L., C. F. Giulivi, and A. G. Ilahude (2003), Deep topographic barriers within the Indonesian seas, *Deep Sea Res., Part II*, *50*, 2205–2228.

Hatayama, T. (2004), Transformation of the Indonesian throughflow water by vertical mixing and its relation to tidally generated internal waves, *J. Oceanogr.*, *60*, 569–585.

Hautala, S., J. L. Reid, and N. A. Bray (1996), The distribution and mixing of Pacific water masses in the Indonesian Seas, *J. Geophys. Res.*, *101*, 12,375–12,390.

Hirst, A. C., and J. S. Godfrey (1993), The role of the Indonesian Throughflow in a global ocean GCM, *J. Phys. Oceanogr.*, *23*, 1057–1086.

Le Provost, C., M. L. Genco, F. Lyard, P. Vincent, and P. Canceil (1994), Spectroscopy of the world ocean tides from a finite element hydrodynamic model, *J. Geophys. Res.*, *99*, 24,777–24,798.

Levitus, S., T. P. Boyer, M. E. Conkright, T. O'Brien, J. Antonov, C. Stephens, L. Stathoplos, D. Johnson, and R. Gelfeld (1998), *World Ocean Database 1998*, vol. 1: Introduction, *NOAA Atlas NESDIS 18*, 346 pp., NOAA, Silver Spring, Md.

Molcard, R., M. Fieux, and A. G. Ilahude (1996), The Indo-Pacific Throughflow in the Timor Passage, *J. Geophys. Res.*, *101*, 12,411–12,420.

Molcard, R., M. Fieux, and F. Syamsudin (2001), The Throughflow within Ombai Strait, *Deep Sea Res., Part I*, *48*, 1237–1253.

Robertson, R., and A. Ffield (2005), M_2 baroclinic tides in the Indonesian Seas, *Oceanography*, *18*, 62–73.

Schiller, A. (2004), Effects of explicit tidal forcing in an OGCM on the water-mass structure and circulation in the Indonesian throughflow region, *Ocean Modell.*, *6*, 31–49.

St. Laurent, L. C., H. L. Simmons, and S. R. Jayne (2002), Estimating tidally driven mixing in the deep ocean, *Geophys. Res. Lett.*, *29*(23), 2106, doi:10.1029/2002GL015633.

Van Aken, H. M., J. Punjanan, and S. Saimima (1988), Physical aspects of the flushing of the east Indonesian basins, *Neth. J. Sea Res.*, *22*, 315–339.

Wajsowicz, R. C., and E. K. Schneider (2001), The Indonesian throughflow's effect on global climate determined from the COLA coupled climate system, *J. Clim.*, *14*, 3029–3042.

P. Bouruet-Aubertot, A. Koch-Larrouy, G. Madec, and R. Molcard, Laboratoire d'Océanographie et du Climat, Laboratoire d'Océanographie Dynamique et de Climatologie, boite 100 4 place Jussieu, F-75252 Paris, France. (akllod@lodyc.jussieu.fr)

T. Gerkema, Royal Netherlands Institute for Sea Research, P.O. Box 59, NL-1790 AB Den Burg, Netherlands.

L. Bessières, Laboratoire d'Etudes en Géophysique et Océanographie Spatiale, 18, av. Edouard Belin, F-31401 Toulouse cedex 9, France.